Electrical Power and Energy Systems 35 (2012) 180–185

Contents lists available at SciVerse ScienceDirect

Electrical Power and Energy Systems

journal homepage: www.elsevier.com/locate/ijepes

Comprehensive study of mixed eccentricity fault diagnosis in induction motors using signature analysis

B.L. Rajalakshmi Samaga *, K.P. Vittal

Department of Electrical and Electronics Engineering, National Institute of Technology Karnataka, Srinivasanagar 575 025, Surathkal, DK, Karnataka, India

ARTICLE INFO

Article history:
Received 18 March 2011
Received in revised form 12 September 2011
Accepted 10 October 2011
Available online 12 November 2011

Keywords:
Eigen value
Modeling
Modified Winding Function Theory
Simulation
Motor Current Signature Analysis (MCSA)
PSD analysis

ABSTRACT

Modeling and simulation studies of an induction motor always help in identifying the parameter to characterize the asymmetrical fault in the machine. Hence in this paper, an air gap eccentric induction motor is modeled using multiple coupled circuit approach and 2D-Modified Winding Function Theory. The machine model is simulated under different eccentricity conditions to obtain the motor current spectra, power spectra and power factor spectra to detect the eccentricity related frequency components and the results are compared. All these analysis are based on the variation in the amplitude of mixed eccentricity related frequency component in these parameters with the variation in the level of eccentricity in the machine. A new fault severity detection method based on co-variance analysis is presented to predict the degree of deterioration in the health of the machine due to air gap eccentricity from the installation stage.

1. Introduction

Recently, condition monitoring unit for induction motor has become an essential component in industrial drives. Among the non-invasive methods of condition monitoring, vibration monitoring is the most popular method used for fault diagnosis in an induction motor. William Thomson says that the number of case histories where vibration monitoring has actually detected broken rotor bars in induction motors is minimal [1]. In the same paper, he has presented case histories in which Motor Current Signature Analysis (MCSA) is successfully used to detect broken rotor bar and eccentricity faults in induction motors. It is reported that they were able to detect the air gap eccentricity fault in the machines successfully by using Eq. (1) and MCSA, when vibration analysis failed to do so.

$$f_e = f_1((1-s)/p \pm n_{ws}) \pm f_1(1-s)/p \tag{1}$$

where f_1 is the supply frequency in Hz, R the number of rotor slots, n_{ws} = 1, 3, 5… = eccentricity integer, s the slip and p is the number of pole pairs.

Nandi et al. [2] report that mixed eccentricity (both static and dynamic eccentricity co exist) characteristic low frequency components near the fundamental in the stator current spectra can be detected by using Eq. (2) which is valid for any combination of machine pole pairs and rotor slot number in a machine.

$$f_e = |f_1 \pm k f_r|, \quad k = 1, 2, 3 \ldots\ldots\ldots \tag{2}$$

where $f_r = f_1(1-s)/p$ is the rotational frequency in Hz.

In the same paper, it has been reported that these low frequency components can give rise to high frequency components described by Eq. (3) which is the more generalized form of Eq. (1) [2].

$$f_e = f_1[(kR \pm n_d)(1-s)/p \pm v] \tag{3}$$

where n_d = 0 in case of static eccentricity, n_d = 1, 2, 3……., in case of dynamic eccentricity (n_d is known as eccentric order), k the integer = 1, 2, 3…. and v is the stator harmonics present in the power supply driving the motor = ±1, ±3, ±5.

It is also been mentioned that these components are strong only for the machines whose pole pairs and rotor slot numbers are related by a specific relation as illustrated in paper [2]. Hence Eq. (3) cannot be used for mixed air gap eccentricity fault detection by MCSA for all kinds of induction motors.

In paper [3], authors have modeled an air gap eccentric machine using Finite Element Method (FEM) and have shown that the amplitude of eccentricity related side band frequency components around the base frequency (refer Eq. (2)) can be used to predict the presence of mixed air gap eccentricity conditions in the machine and have validated the simulation results experimentally. But they

* Corresponding author.
E-mail addresses: rajisamaga@yahoo.com (B.L. Rajalakshmi Samaga), vittal_nitk@yahoo.com (K.P. Vittal).

0142-0615/$ - see front matter © 2011 Elsevier Ltd. All rights reserved.
doi:10.1016/j.ijepes.2011.10.011

have expressed apprehensions regarding the effect of noise on this type of detection method.

Recently, some researchers have tried other signature analysis such as instantaneous power, instantaneous power factor and instantaneous torque signature analysis for eccentricity fault detection in induction motors. M'hamed Drif and Marques Cardoso [4], have made use of instantaneous power spectrum for the detection of mixed air gap eccentricity fault in the machine and have shown by both simulation as well as experimentally that the amount of information carried by total instantaneous power is higher than the one extracted from the motor current alone. Same authors have shown that instantaneous power factor signature analysis is another method which can be used for mixed eccentricity fault detection in the motors [5].

Fast Fourier Transform (FFT) and Power Spectral Density (PSD) are the most commonly adopted frequency analysis tools for eccentricity detection by MCSA as stator current is considered to be stationary [2,3,6–8]. But in reality, stator current signals turns out to be non stationary as they are affected by power supply changes and load fluctuations. Hence, many researchers have introduced new techniques such as Short Time Fourier Transform (STFT), Wavelet Transform (WT), Wavelet Packet Transform (WPT). to identify the eccentricity related frequency components in the stator current [9–12]. Recently artificial intelligence methods such as Neural Networks, Fuzzy logic, and Genetic Algorithms so on are used for asymmetrical fault detection in the machine [13,14]. As the increase in the non uniformity of air gap is a very slow process, time information from the current signal is not of great concern in the asymmetrical fault detection process. Hence in this paper, detection of eccentricity characteristic harmonics in the stator current is restricted to only frequency analysis (PSD analysis).

In this study, a dynamic model of an induction motor having mixed eccentricity fault is developed and simulated for a particular inclined static eccentricity condition. PSD analysis is performed on the instantaneous stator phase A current, instantaneous power and instantaneous power factor to identify the eccentricity characteristic harmonics in them and obtained results are compared. Air gap eccentricity exists even in a newly manufactured machine. This can increase the Unbalanced Magnetic Pull (UMP) on the rotor resulting in further deterioration in the health of the machine. In order to access the degree of increase in the air gap eccentricity in the machine, a new technique based on Eigen value is proposed in this paper.

Section 2, gives the modeling details of a three phase induction motor suffering from inclined mixed air gap eccentricity condition. MCSA is conducted on the stator current samples obtained by simulating the model for different eccentricity conditions and its results are given in Section 3. Similar analysis is conducted on the extracted power and power factor data samples obtained by simulation and observations are presented in Sections 4 and 5 respectively. In Section 6, a new fault severity index is defined by performing the true eigenvector-based multivariate analysis on the MCSA results and is followed by conclusion in Section 7.

2. Modeling and simulation of three phase induction motor

Three phase squirrel cage induction motor is modeled using multiple coupled circuit approach and 2D-Modified Winding Function Theory (2D-MWFT) [15–19] because

(i) it can take into account of eccentricity fault in the machine,
(ii) skewing of rotor can be accounted in the model,
(iii) inclined eccentricity can be incorporated in the model.

The induction motor details and stator phase A and rotor loop1 turn functions are given in Appendices A.1 and A.2. The mutual inductance between the windings (L_{ij}) (between stator phase and rotor loop, between rotor bars and between stator phases) is calculated using numerical integration method. The axial length along the rotor is divided into 11 sections (z) and for each section, mutual inductance between the windings '*i*' and '*j*' for every rotor position (θ_r) is calculated by using the formula [19].

$$L_{ij}(\theta_r, z) = 2\pi\mu_0 r\ell[\langle Pn_i n_j\rangle - (\langle Pn_i\rangle\langle Pn_j\rangle/\langle P\rangle)](\ell/11) \quad (4)$$

where L_{ij} is the mutual inductance between the windings '*i*' and '*j*' in *H*, *z* the the section along the axial length of rotor, n_i the turn function of winding '*i*', n_j the turn function of winding '*j*', μ_0 the absolute permeability, *r* is the average radius of air gap in m, ℓ is length of stack in m and *P* is the permeance of air gap in m^{-1}.

The sum of inductances calculated for every section along the axial length for a given rotor position gives the mutual inductance between the windings for that rotor position and is calculated by using (5).

$$L_{ij}(\theta_r) = \sum_{z=1}^{z=11} L_{ij}(\theta_r, z) \quad (5)$$

The permeance *P* is calculated by using the static eccentricity index (δ_s) and dynamic eccentricity index (δ_d) as given in Eq. (6) [18,19].

$$P(\phi, z, \theta_r) = P_0(z) + P_1(z)\cos(\phi - \rho(z)) + P_2(z)\cos(2\phi - 2\rho(z)) \quad (6)$$

where p_0, p_1, p_2 and ρ are calculated as

$$P_0(z) = \frac{1}{g_0}$$

$$P_1(z) = 2\left[\frac{1}{g_0\sqrt{1-\delta^2(z)}}\right]\left[\frac{\left(1-\sqrt{1-\delta^2(z)}\right)}{\delta(z)}\right]$$

$$P_2(z) = 2\left[\frac{1}{g_0\sqrt{1-\delta^2(z)}}\right]\left[\frac{\left(1-\sqrt{1-\delta^2(z)}\right)}{\delta(z)}\right]^2$$

$$\rho(z) = \tan^{-1}\left(\frac{\delta_d(z)\sin(\theta_r)}{\delta_s(z) + \delta_d(z)\sin(\theta_r)}\right)$$

$$\delta(z) = \sqrt{\delta_s^2(z) + \delta_d^2(z) + 2\delta_s(z)\delta_d(z)\cos(\theta_r)}$$

where δ is the mixed eccentricity index and ϕ is the rotor circumferential angle.

The machine is modeled to have mixed eccentricity, i.e. 5% dynamic eccentricity and inclined static eccentricity of 20% at one end and 35% on the other end. The variation of static eccentricity index along the rotor length is calculated by using (7)

$$\delta_s(z) = \delta_{s0} + kz \quad (7)$$

where δ_{s0} is the static eccentricity at one end and *k* is the slope with which rotor is inclined.

The model is developed by using the machine details given in Appendix B and it is capable of starting with full load on it. It responds very well to the load fluctuations in the machine. The variation of mutual inductance between stator phase A and rotor loop1, rotor loop1 and rotor loop2 and stator phase A and stator phase B obtained for different rotor positions (θ_r) are as shown in Fig. 1. The machine model with full load on it is simulated at a fixed step size of 0.00005 using Runge–Kutta 4 method. 20,000 samples of instantaneous stator current, instantaneous power and instantaneous power factor at sampling frequency of 20 kHz are extracted

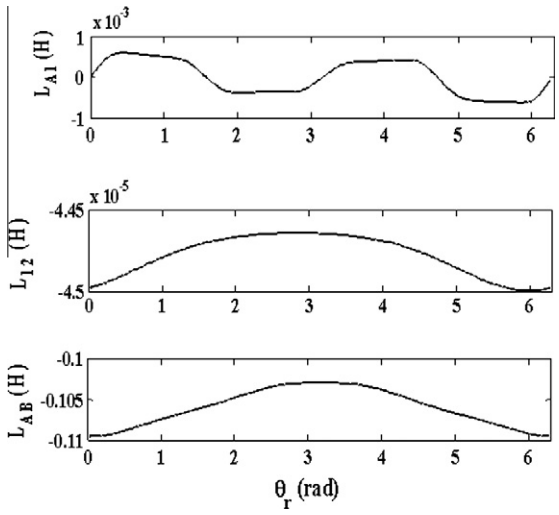

Fig. 1. Mutual inductance between stator phase A and rotor loop1, rotor loop1 and rotor loop2, stator phase A and phase B.

and are filtered through a low pass filter using Hann window designed for a cut off frequency of 10 kHz. The filtered data are stored for frequency analysis whose details are given in Sections 3–6.

3. Motor current signature analysis

Power Spectral Density (PSD) analysis is conducted on the stator phase A current samples obtained by simulating the model for the mixed eccentricity condition of 5% dynamic eccentricity and inclined static eccentricity of 20% at one end and 35% on the other end and the resulting current spectra is shown in Fig. 2. The chosen frequency resolution to obtain the current spectra is 1 Hz. Presence of mixed air gap eccentricity condition prevailing in the machine can be detected by the side band frequency components (Lower Side Band (LSB) and Upper Side Band (USB)) around the base frequency in the stator current spectra as described by the Eq. (2).These low frequency components can give rise to high frequency components as given in Eq. (3). For the machine chosen for analysis, these high frequency components in the stator current are found to be weak. Hence, only side band eccentricity characteristic frequency components around the fundamental are detected in the stator phase current spectra obtained by PSD analysis. They are $(f_1 - f_r)$ (LSB) and $(f_1 + f_r)$ (USB) values and found to be at 26 Hz and 74 Hz respectively in the stator phase A current spectra. The steady state speed of the machine is found to be148 rad/s

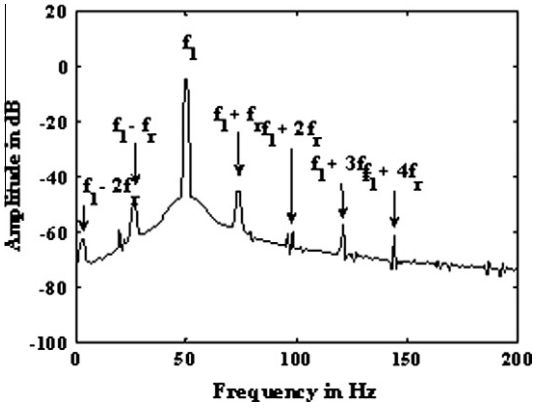

Fig. 2. Stator current spectra for $\delta_d = 0.05$.

Table 1
$(f_1 - f_r)$ and $(f_1 + f_r)$ frequency components and their amplitude in stator phase A current spectra.

DE index	$(f_1 - f_r)$, amplitude in dB		$(f_1 + f_r)$, amplitude in dB	
0.05	26	−56.80	74	−54.32
0.1	26	−50.85	74	−48.24
0.15	26	−47.06	74	−44.59
0.2	26	−44.37	74	−41.82
0.25	26	−42.52	74	−39.41
0.3	26	−41.98	74	−37.09

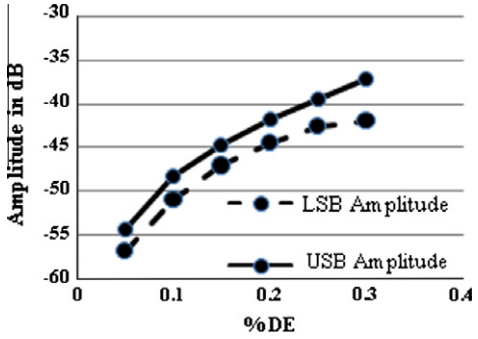

Fig. 3. Variation of side band frequency component's amplitude in stator current spectrum.

$(s = 0.0584)$. Theoretical values of $(f_1 - f_r)$ and $(f_1 + f_r)$ calculated by using Eq. (2), are found to be 26.46 Hz and 73.54 Hz. respectively.

The variation in the degree of mixed eccentricity can be achieved in three ways

(i) By keeping the static eccentricity constant and varying the dynamic eccentricity.
(ii) By keeping the dynamic eccentricity constant and varying the static eccentricity.
(iii) By varying both the static eccentricity and the dynamic eccentricity.

If the rotor-shaft assembly is sufficiently stiff, the level of static eccentricity does not change [2]. In this study, data of a 3 hp machine having rigid rotor-shaft assembly is considered for modeling. For the above said reason, simulations are carried out for the condition in which the static eccentricity index is kept constant and the dynamic eccentricity index is varied.

Table 1 shows the eccentricity related frequency components obtained by PSD analysis for the condition of inclined static eccentricity of 20% at one end and 35% on the other end with dynamic eccentricity values being varied. The frequency resolution is 1 Hz. The variation of amplitudes of lower side band frequency (LSB) and upper side band frequency components (USB) around the base frequency are shown in Fig. 3.

From Table 1 and Fig. 3, it is inferred that with the increase in dynamic eccentricity (mixed eccentricity), amplitudes of mixed eccentricity related frequency components also increase. The frequency at which these components exist remains the same as the change in slip is very small at different eccentric conditions and hence not noticeable.

4. Instantaneous power signature analysis

The instantaneous power is calculated by using the Eq. (8) [20].

$$p_{\text{phasor}} = (v_a - v_0)(i_a - i_0) + (v_b - v_0)(i_b - i_0) + (v_c - v_0)(i_c - i_0) \quad (8)$$

where $v_0 = (v_a + v_b + v_c)/3$,
$i_0 = (i_a + i_b + i_c)/3$
and v_a, v_b and v_c are the instantaneous phase voltages, i_a, i_b and i_c are the instantaneous phase currents.

Eq. (8) is selected as compared to the classic instantaneous power measurement equation because it is in more generalized form and is valid for both balanced and unbalanced supply voltage conditions. In the instantaneous power signature spectrum, besides the fundamental and the two sideband components at $(2f_1 - f_r)$ and $(2f_1 + f_r)$, it contains an additional component at the modulation frequency f_r [4]. The instantaneous power spectrum obtained from simulating the machine model for the eccentricity condition of 5% dynamic eccentricity and inclined static eccentricity of 20% at one end and 35% at the other end is as shown in Fig. 4. From the power spectrum, eccentricity characteristic harmonics, f_r, $(2f_1 - f_r)$ and $(2f_1 - 2f_r)$ are found at 24 Hz, 76 Hz and 53 Hz respectively. Theoretically, they are at 23.54 Hz, 76.46 Hz and 52.92 Hz.

Inclined static eccentricity of 20% at one end and 35% at the other end is maintained constant and dynamic eccentricity is varied in the model during simulation and amplitudes of eccentricity characteristic frequency components are computed. The variation in the amplitudes of f_r, $(2f_1 - f_r)$ and $(2f_1 - 2f_r)$ frequency components in the power spectra with the variation in dynamic eccentricity is shown in Table 2 and Fig. 5.

From Table 2 and Fig. 5, it is concluded that with the increase in the eccentricity level in the machine, amplitudes of eccentricity related harmonic components also increase. From the power spectra, it can be inferred that the variation in the amplitude of eccentricity characteristic harmonics with the variation in mixed eccentricity level is higher as compared to the current spectra.

5. Instantaneous power factor signature analysis

Flux distribution in the air gap of induction motor gets affected with the non uniformity in the air gap. Power factor is the primary factor to get affected by the unequal distribution of flux in the air gap. The instantaneous power factor, $\cos(\Phi)$ is defined by the ratio of the active and the apparent instantaneous powers [20].

$$\cos(\phi) = p_{\text{phasor}}/S_{\text{phasor}} \quad (9)$$

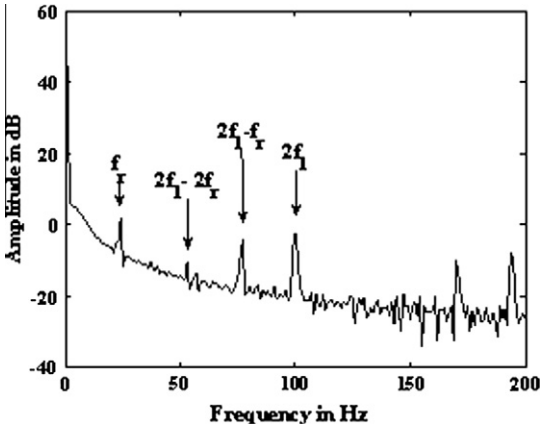

Fig. 4. Instantaneous power spectra for $\delta_d = 0.05$.

Table 2
f_r, $(2f_1 - f_r)$ and $(2f_1 - 2f_r)$ frequency components and their amplitude in power spectra.

DE index	f_r, amplitude in dB		$(2f_1 - f_r)$, amplitude in dB		$(2f_1 - 2f_r)$, amplitude in dB	
0.05	24	−0.84	76	−6.17	53	−16.40
0.1	24	5.54	76	−0.13	53	−8.89
0.15	24	9.02	76	4.03	53	−1.79
0.2	24	11.88	76	6.94	53	3.56
0.25	24	14.43	76	9.72	53	8.01
0.3	24	17.25	76	12.15	53	11.59

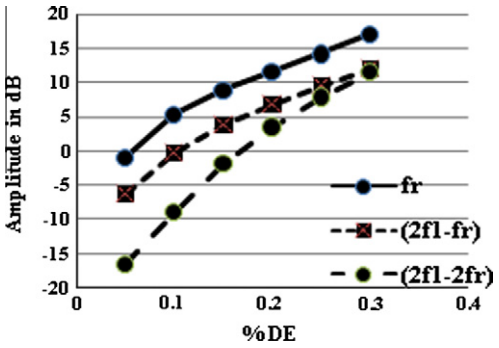

Fig. 5. Variation of eccentric related frequency component's amplitude in power spectrum.

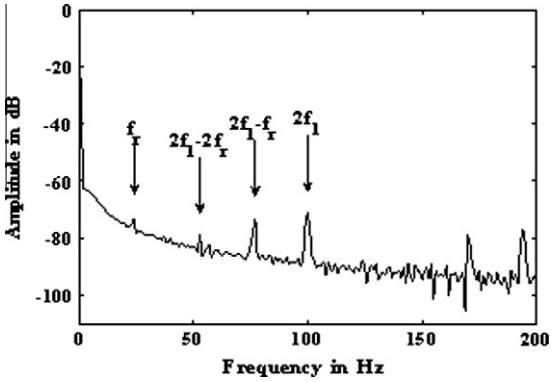

Fig. 6. Instantaneous power factor spectra.

Table 3
f_r, $(2f_1 - f_r)$ and $(2f_1 - 2f_r)$ frequency components and their amplitude in power factor spectra.

DE index	f_r, amplitude in dB		$(2f_1 - f_r)$, amplitude in dB		$(2f_1 - 2f_r)$, amplitude in dB	
0.05	24	−80.13	76	−74.91	53	−85.51
0.1	24	−73.63	76	−68.91	53	−77.58
0.15	24	−70.78	76	−64.63	53	−70.39
0.2	24	−67.88	76	−61.62	53	−64.99
0.25	24	−63.91	76	−58.71	53	−60.37
0.3	24	−57.92	76	−56.23	53	−56.65

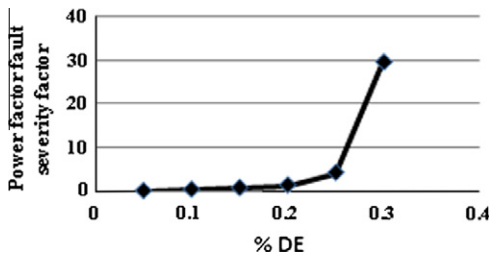

Fig. 7. Power factor severity factor vs %DE.

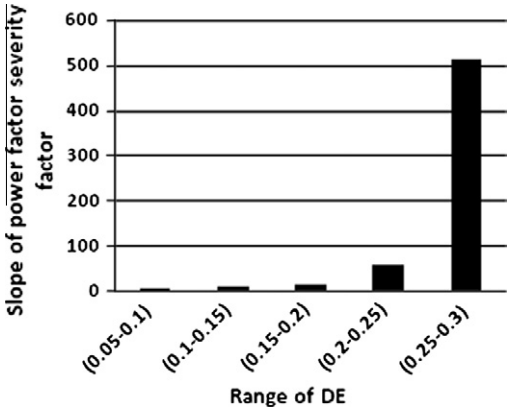

Fig. 8. Slope of power factor severity factor.

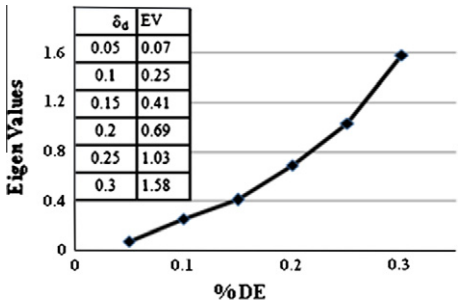

Fig. 9. Variation of Eigen values.

where s_{phasor} is the three-phase instantaneous apparent power and the product of 3 times the rms voltage and current and is defined as

$$S_{phasor} = 3VI/2 \tag{10}$$

where $V = \sqrt{2}\sqrt{((v_a - v_0)^2 + (v_b - v_0)^2 + (v_c - v_0)^2)/3}$

$I = \sqrt{2}\sqrt{((i_a - i_0)^2 + (i_b - i_0)^2 + (i_c - i_0)^2)/3}.$

Since instantaneous power factor depends on the instantaneous power, the eccentricity related characteristic frequency component f_r which appears in power spectrum is also present in the power factor spectrum. PSD analysis is performed on the filtered instantaneous power factor data samples obtained by simulating the machine model with 20% static eccentricity at one end and 35% at the other end and 5% dynamic eccentricity conditions. The power factor spectrum obtained is as shown in Fig. 6.

Amplitudes of eccentricity related harmonic components f_r (24 Hz), $(2f_1 - f_r)$ (76 Hz) and $(2f_{1.} - 2f_r)$ (53 Hz) varies with the variation in dynamic eccentricity in the machine and is shown in Table 3. From Table 3 it is seen that with the increase in the eccentricity level in the machine, amplitudes of eccentric related characteristic harmonic components also increases.

The authors in paper [5], have defined a power factor fault severity factor as the ratio of the amplitude of the f_r component of the instantaneous power factor of the motor and the corresponding dc value to predict the severity of the fault. The observation made by them is that fault severity factor (ratio) increases with the increase in the air gap eccentricity. Similar results are obtained and are shown in Fig. 7. From the Fig. 7, it can be observed that as the dynamic eccentricity increases in the machine, power factor fault severity factor also increases. Hence, the slope of the power factor severity factor curve is a better fault severity indicator in field applications (refer Fig. 8). From Fig. 8, it is inferred that the slope of the power factor severity curve contains more information about the severity of eccentricity fault in the machine and can be used for fault detection.

6. Fault severity detection by Eigen values

The Eigen values represent the distribution of the source data's energy among each of the Eigen vectors. The cumulative energy content of Eigen vector is the sum of the energy content across all of the Eigen values. The amplitudes of the eccentricity characteristic harmonics f_r, $(f_1 - f_r)$, $(f_1 + f_r)$ components are obtained for different mixed eccentricity conditions and are compared to those obtained under healthy condition. Co-variance matrix is formed from which Eigen values are evaluated. The lowest Eigen values obtained for different eccentricity conditions are plotted as shown in Fig. 9.

From Fig. 9, it is inferred that Eigen values increase with the increase in dynamic eccentricity level in the machine. Hence, it can be used as a fault severity index to predict the degree of mixed eccentricity fault in the machine. This method has an added advantage that severity index is defined by evaluating the amplitudes of many eccentricity related harmonics and these values are compared to those of a healthy machine (or the installation condition of the machine). This index, along with 'Total Indicated Reading (TIR)' or 'total run out' provided by the manufacturer can be used to take a decision whether to send the machine to manufacturer's workshop or not.

7. Conclusion

In this paper, an induction motor suffering from inclined mixed air gap eccentricity is modeled using multiple coupled circuit approach and 2D Modified Winding Function Theory. MCSA, instantaneous power signature analysis, instantaneous power factor signature analysis are conducted on the extracted data samples obtained by simulation of the model. The presence of eccentricity characteristic frequency components in these signatures shows the presence of mixed eccentricity conditions in the machine but does not give any information regarding the severity of the fault. All newly built machines are said to possess small amount of eccentricity due to mechanical reasons. The very presence of this static eccentricity can give rise to Unbalanced Magnetic Pull (UMP) on the rotor resulting in increase of eccentricity level in the machine. This is a cumulative process resulting in the rub between the stator and the rotor. The proposed Eigen value based fault severity detection compares the amplitudes of the frequency components of stator current of an eccentric machine with those of healthy machine condition (condition at the time of installation) and is a better indicator of the deterioration in the health of the machine over a period. It can be used as a tool to predict the degree of air gap eccentricity fault in the machine and hence avoid total failure of the machine.

Acknowledgments

We would like to acknowledge Integrated Electronics Ltd., Bangalore and LARSEN & TOUBRO for providing the machine along with machine parameters.

Appendix A

A.1. Stator phase A turn function (refer Fig. A.1)

A.2. Rotor loop1 turn function (refer Fig. A.2)

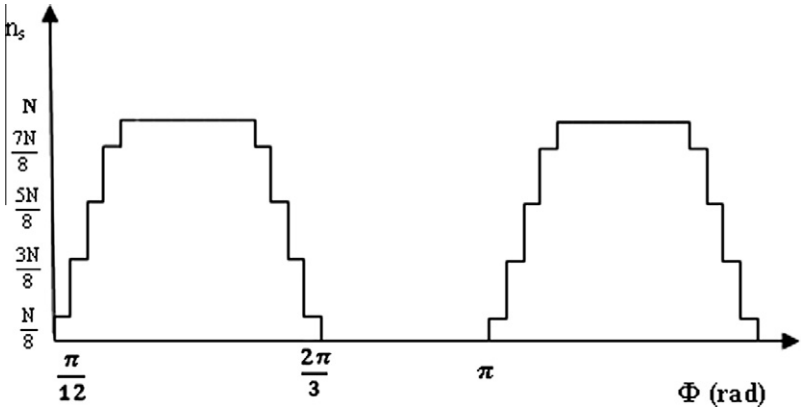

Fig. A.1. Stator phase A turn function.

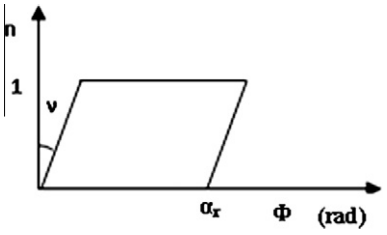

Fig. A.2. Rotor loop 1 turn function.

Appendix B. Machine details

2.2 kW, 3 hp, 400/415 V, 50 Hz, 3ΦAC, 1500 rpm, 4 pole squirrel cage induction motor.

Number of stator slots = 24.
Number of rotor bars = 30.
Length of stacks = 120 mm.
Effective air gap = 0.35 mm.
Mean radius of air gap = 89.65 mm.
Number of turns/phase = 400.
Stator resistance = 7.6 Ω.
Stator leakage inductance = 38.43 mH.
Rotor bar resistance = 0.00376 Ω.
Rotor bar leakage inductance = 44.52 μH.
Rotor end ring segment resistance = 0.0012 mΩ.
Rotor end ring segment inductance = 1.24 μH.
Rotor inertia in GD^2 = 0.024 kg-m^2.

References

[1] William Thomson T. On-line motor current signature analysis prevents premature failure of large induction motor drives. Maint Asset Manage 2009;24(3):30–5.
[2] Nandi Subhasis, Hamid Toliyat A, Xiaodong Li. Condition monitoring and fault diagnosis of electrical motors – a review. IEEE Trans Energy Conver 2005;20(4):719–29.
[3] Faiz Jawad, Ebrahim Bashir Mahdi, Akin Bilal, Hamid Toliyat A. Comprehensive eccentricity fault diagnosis in induction motors using finite element method. IEEE Trans Magnetics 2009;45(3):1764–7.
[4] M'hamed Drif, A.J. Marques Cardoso, Air gap eccentricity fault diagnosis in three phase induction motors by the instantaneous power signature analysis, in: 3rd IET international conference on power electronics, machines and drives, 2006, pp. 349–353.
[5] M'hamed Drif, A.J. Marques Cardoso, Airgap eccentricity fault diagnosis, in three-phase induction motors, using the instantaneous power factor signature analysis, in: 4th IET conference on power electronics, machines and drive, 2008, pp. 587–591.
[6] Gojko Joksimovie M, Momir Durovic D, Penman J, Neil Arthur. Dynamic simulation of dynamic eccentricity in induction machines – winding function approach. IEEE Trans Energy Conver 2000;15(2):143–8.
[7] Xiaodong Li, Qing Wu, Nandi S. Performance analysis of a three phase induction machine with inclined static eccentricity. IEEE Trans Ind Appl 2007;43(2):531–41.
[8] Sahraoui M, Ghoggal A, Zouzou SE, Benbouzid ME. Dynamic eccentricity in squirrel cage induction motors – Simulation and analytical study of its spectral signatures on stator currents. Simulat Model Practice Theory 2008;16:1503–13.
[9] H. Hamidi, A.R. Nasiri, F. Taringoo, Detection and isolation of mixed eccentricity in three phase induction motor via wavelet packet decomposition, in: 5th Asian control conference, 2004, pp. 1371–1375.
[10] Cusido Jordi, Romeral Luis, Ortega Juan A, Rosero Javier A, Espinosa Antonio Garcia. Fault detection in induction machines using power spectral density in wavelet decomposition. IEEE Trans Ind Electron 2008;55(2):633–43.
[11] Niu Gang, Widodo Achmad, Son Jong-Duk, Yang Bo-Suk, Hwang Don-Ha, Kang Dong-Sik. Decision-level fusion based on wavelet decomposition for induction motor fault diagnosis using transient current signal. Sci Direct – Expert Syst Appl 2008;35:918–28.
[12] Antonino-Daviu J, Jover P, Rieraa M, Arkkiob A, Roger-Folcha J. DWT analysis of numerical and experimental data for the diagnosis of dynamic eccentricities in induction motors. Mech Syst Signal Process 2007;21:2575–89.
[13] Tan SC, Lim CP, Rao MVC. A hybrid neural network model for rule generation and its application to process fault detection and diagnosis. Eng Appl Artif Int 2007;20:203–13.
[14] Lei Yaguo, He Zhengjia, Zi Yanyang, Hu Qiao. Fault diagnosis of rotating machinery based on multiple ANFIS combination with Gas. Mech Syst Signal Process 2007;21:2280–94.
[15] Toliyat Hamid A, Lipo Thomas A. Transient analysis of cage induction machines under stator, rotor bar and end ring faults. IEEE Trans Energy Conver 1995;10(2):241–7.
[16] Toliyat Hamid A, Arefeen Mohammed S, Parlos Alexander G. A method for dynamic simulation of air-gap eccentricity in induction machines. IEEE Trans Ind Appl 1996;32(4):910–8.
[17] Guillermo Bossio, Cristian De Angelo, Guillermo Garcia, Jorge Solsona, Maria Ines Valla, A 2D model of the induction motor: an extension of the modified winding function approach, in: Proceedings of 28th annual conference of the IEEE industrial electronics society, IECON, 2002, pp. 62–67.
[18] A. Ghoggal, A. Aboubou, S.E. Zouzou, M. Sahraoui, H. Razik, Considerations about the modeling and simulation of airgap eccentricity in induction motors, in: Proceedings of IEEE IECON conference, Paris, France, 2006, pp. 4987–4992.
[19] Rajalakshmi Samaga BL, Vittal KP. A simplified modeling approach for accounting skewing effect in rotor bars of squirrel cage induction motor and its application in motor inductance calculation. J Electr Eng, Romania 2010;10:178–83.
[20] S. Hsu, John, Instantaneous power factor determined by instantaneous phasors, a document from the department of energy's information bridge: DOE scientific and technical information web site, 1998.